Published in: Journal of cerebral blood flow and metabolism (2002), vol. 22, iss. 6, pp. 753-765
Status: Postprint (Author's version)

Modeling [^{18}F]MPPF Positron Emission Tomography Kinetics for the Determination of 5-Hydroxytryptamine(lA) Receptor Concentration With Multisection

*Nicolas Costes, *$ Isabelle Merlet, *Luc Zimmer, *Franck Lavenne, *Luc Cinotti, #Jacques Delforge, §André Luxen, *Jean-François Pujol, and *Didier Le Bars

**Centre d'Exploration et de Recherche Médicales par Emission de Positons, Lyon, France, $Lyon Federative Institut of Neurosciences, Claude Bernard University, Lyon, France, #SHFJ, Commissariat a l'Energie Atomique, Orsay, France, and §CRC, Université de Liège, Belgium*

Abstract

The selectivity of [^{18}F]MPPF (fluorine-18-labeled 4-(2' -methoxyphenyl)-1 -[2' -(N-2"-pirydynyl)-p-fluorobenza-mido]ethylpiperazine) for serotonergic 5-hydroxytrypta-mine(lA) (5-HT_{1A}) receptors has been established in animals and humans. The authors quantified the parameters of ligand-receptor exchanges using a double-injection protocol. After injection of a tracer and a coinjection dose of [^{18}F]MPPF, dynamic positron emission tomography (PET) data were acquired during a 160-minute session in five healthy males. These PET and magnetic resonance imaging data were coregistered for anatomical identification. A three-compartment model was used to determine six parameters: F_v (vascular fraction), K_1, k_2 (plasma/free compartment exchange rate), k_{off}, k_{on}/V_r (association and dissociation rate), B_{max} (receptor concentration), and to deduce K_d (apparent equilibrium dissociation rate). The model was fitted with regional PET kinetics and arterial input function corrected for metabolites. Analytical distribution volume and binding potential were compared with indices generated by Logan-Patlak graphical analysis. The $5HT_{1A}$ specificity for MPPF was evidenced. A B_{max} of 2.9 pmol/mL and a K_d of 2.8 nmol/L were found in hippocampal regions, K_d and distribution volume in the free compartment were regionally stable, and the Logan binding potential was linearly correlated to B_{max}. This study confirms the value of MPPF in the investigation of normal and pathologic systems involving the limbic network and 5-HT_{1A} receptors. Standard values can be used for the simulation of simplified protocols.

Key Words: Serotonin-ergic 5-HT_{1A} receptors—Compartmental model—[^{18}F]MPPF— Positron emission tomography.

Serotonin is involved in the neuromodulation and neurotransmission of the mammalian nervous system and can modify a large variety of physiologic responses through multiple subtypes of receptors. Among the 17 subtypes of receptors identified to date, 5-hydroxytrypta-mine(lA) (5-HT_{1A}) is currently the most studied (Per-outka, 1995).

The involvement of 5-HT_{1A} serotonergic receptors in neurophysiologic and psychiatric disorders has been revealed in both the animal and human brain by autoradiographic postmortem studies. Abnormalities in 5-HT_{1A} receptor densities were found in the brains of patients with depression, dementia, and schizophrenia (Cowen, 2000). In addition, serotonin implication in epileptic seizure control via the 5-HT_{1A} receptors has been evidenced in rats (Statnick et al., 1996; Wada et al., 1997). Moreover, abnormal serotonin concentrations were found *ex vivo* in resected samples of cortex in epileptic patients (Louw et al., 1989; Pintor et al., 1990), and a decrease of 5-HT synthesis in epileptic areas was evidenced *in vivo* by PET using [^{18}F]AMT (Chugani et al., 1998).

Using positron emission tomography (PET), several carbonyl and fluoryl radioligands have been developed recently that allow for the *in vivo* quantification of 5-HT_{1A} receptors (Cliffe, 2000). [^{11}C]N(2-(4-(2-meth-oxyphenyl)-1 -piperazinyl)ethyl)-N-(2-pirydynyl) cyclo-hexanecarboxamide ([^{11}C]WAY 100635) is an antagonist of the 5-HT_{1A} receptors. Delineation (Pike et al., 1995; Pike et al., 1996) and quantification (Farde et al., 1998; Gunn et al., 1998) studies showed a specificity and high affinity of [^{11}C]WAY 100635 for 5-HT_{1A} receptors. These studies confirmed that 5-HT_{1A} receptors are located mainly in the limbic system, but are also present in the entorhinal and cingular cortex. However, WAY 100635 presents a much higher affinity (0.8 nmol/L) than serotonin to its own 5-HT_{1A} receptors (Ki = 4.7 nmol/L). Consequently, recent studies suggest that this ligand may not be the most suitable tool to study endogenous variations of serotonin concentration (Hume et al., 2001). The radiosynthesis of another PET tracer antagonist to the 5-HT_{1A}, 4-(2'-methoxyphenyl)-l-[2'-(N-2'-pirydynyl)-p-fluorobenzamido]ethylpiperazine (MPPF), was recently optimized and simplified (Le Bars et al.,

1998). This tracer is an analogue of WAY 100635, labeled with fluorine-18 ([^{18}F]MPPF). *In vivo* and *ex vivo* distribution studies in the rat (Plenevaux et al., 2000*b*) and cat brain (Ginovart et al., 2000; Le Bars et al, 1998) confirmed a selective binding of the molecule in cerebral regions rich in 5-HT$_{1A}$ receptors such as the dorsal raphe nuclei, hippocampus, cingular gyrus, or septum, and with less intensity in the neocortex (Plenevaux et al., 2000*a*). An initial examination of [^{18}F]MPPF in healthy human volunteers showed a similar distribution (Passchier et al., 2000*a*). A recent analysis performed with a simplified method (quantification of binding relative to a reference tissue region) showed a good cerebellum-to-target-region ratio. This magnitude decreased by 40% after a blocking dose of pindolol, a competitive antagonist of 5-HT$_{1A}$ receptors (Passchier et al., 2000*b*). These preliminary results, together with the longer half-life of ^{18}F compared with [^{11}C] WAY 100635 and the lower affinity of MPPF for 5-HT$_{1A}$ receptors (Ki = 3.3 nmol/L; Zhuang et al., 1994), emphasize the potential use of this ligand as a radiopharmaceutical for quantitative studies of the serotonergic 5-HT$_{1A}$ system *in vivo*.

The aim of the present study was to perform a complete modeling of the *in vivo* kinetics of [^{18}F]MPPF, including parameter estimation of (1) the transport from plasma to tissue, and (2) the specific binding of the ligand to the 5-HT$_{1A}$ receptors. We used a multiple-injection protocol (Delforge et al., 1990) to estimate six parameters (vascular fraction, exchange rates, and receptor density) that in return were used to validate simplified quantitative methods.

MATERIALS AND METHODS

[^{18}F]MPPF synthesis

[^{18}F]MPPF was obtained by nucleophilic fluoration on a nitro precursor with a radiochemical yield of 20% to 25% EOS and a specific activity of 37 to 111 GBq/µmol. (Le Bars et al., 1998; Le Bars et al., 2001).

Experimental protocol

Subjects. Five healthy male volunteers (21-30 years) participated in the study. A medical interview and the inspection of the anatomical T_1 magnetic resonance (MR) image revealed that none of subjects had psychiatric or neurological illnesses. Subjects gave their informed consent to the protocol approved by the local ethical committee in accordance with the declaration of Helsinki. Subject's participation involved an MR imaging and a PET session.

Magnetic resonance imaging session. The MR imaging acquisition consisted of a three-dimensional anatomical T_1-weighted sequence on a 1.5-T Siemens Magnetom scanner (Siemens AG, Erlangen, Germany). The anatomical volume covered the whole brain with millimeter cubic voxels.

Positron emission tomography session. The PET session was performed on a CTI-Siemens HR+ (Knoxville, TN, U.S.A.) during the afternoon. Before the session, subjects received 330 mL water and a standardized meal (prepared by a dietetics unit) to normalize dietary input before the PET examination, and then were laid supine on the bed of the PET scanner. For blood sampling, a catheter was placed in the radial artery of the right arm using local anesthesia. For tracer injections, a second intravenous catheter was placed in radial vein of the left arm. For each subject a thermoformable head holder was molded to limit head movements during acquisition. Subjects were positioned in the PET scanner so that the crossed laser beam delimiting the axial field of view (15.2 cm) covered the brain. Before emission acquisition, a 10-minute transmission scan was performed using three ^{68}Ge rod sources for the measurement of tissue and head support attenuation.

Multiinjection protocol consisted of two [^{18}F]MPPF bolus injections of 185 ± 9 MBq. The injections were performed at a mean interval of 88.5 ± 4.2 minutes. At time zero, the synthesis of [^{18}F]MPPF was calibrated to a mean specific activity of 37 GBq/µmol. The first syringe contained a tracer dose of [^{18}F]MPPF, whereas the second syringe was prepared by dilution with unlabeled MPPF to obtain a 10-times lower specific activity 80 minutes later (see Table 1 for details regarding concentrations and timing).

Two dynamic PET scans of emission were acquired to evaluate the local radiotracer concentration during the 70-minute period after each injection. Dynamic scans comprised 37 frames of increasing duration (20 seconds to 5 minutes), and a total of 74 frames were analyzed. The PET scanner was operating in three-dimensional mode. Images were corrected for scatter and attenuation and were reconstructed using a filtered back projection (Hamming filter of cut-off 0.5 cycles/pixels) to provide a three-dimensional volume comprising 63 slices (2.42-mm thickness), with 128 x 128 voxels in plane (2.06 x 2.06 mm). In the center of the field of view, National Electrical Manufacturers Association protocol measured an nominal axial resolution of 4.1 mm and a nominal

transverse resolution of 4.4 mm for a point source reconstruct with ramp filter (Brix et al., 1997).

Throughout the experiment, arterial blood samples were collected at different intervals after injection (12x15,3x30, and 6 x 60 seconds, and 6x5 minutes). In general, 0.7 mL blood was withdrawn except at 2, 5 10, 15, 20, 30, 40, 60, or 70 minutes after injection, at which time 2.5 mL blood was collected to measure metabolite concentration. Blood samples were rapidly centrifuged, and the plasma was separated and assessed for radioactivity with an automated γ counter. In parallel, a plasma aliquot was denatured by acetonitrile containing a carrier amount of cold MPPF. Analytical high-pressure liquid chromatography was then performed on samples with radioactivity counting of the collected fractions.

TABLE 1. *Numerical value of the experimental positron emission tomography multiinjection protocol parameters*

	Tracer injection, time 0					Coinjection			
Subject	**Dose (MBq)**	**Specific radioactivity (GBq/µmol)**	**Labeled dose (nmol)**	**Unlabeled dose (nmol)**	**Time (min)**	**Dose (MBq)**	**Labeled dose (nmol)**	**Unlabeled dose (nmol)**	**Apparent specific radioactivity (GBq/µmol)**
1	203	33	6.1	0	87	170	5.1	52.3	3.0
2	199	37	5.38	0	94	184	5.0	44.8	3.7
3	190	37	5.14	0	84	195	5.3	47.4	3.7
4	185	37	5	0	89	192	5.2	74.6	2.6
5	191	24	7.94	0	80	180	7.48	196.2	1.0

Dose and specific activities are measured at the injection time.

Data analysis

Arterial function analysis. After correction for the decay of ^{18}F, time-activity curves of total blood and plasma were extracted and converted to time-concentration curves indicating the specific radioactivity of [^{18}F]MPPF. We evaluated the fraction in the plasma curve of nonmetabolized MPPF at different sampling times. The mean curve of the data regarding our five subjects was fitted in a least-square sense to a biexponential function (Levenberg-Marquardt method). For each subject we obtained the input function of the ligand in the vascular network by multiplying the time-concentration curves of plasma by the fitted unmetabolized fraction of [^{18}F]MPPF.

Image processing. From two dynamic acquisitions of 37 frames, we computed a static image of equilibrium from 20 to 70 minutes after injection. To correct for possible head movements, these static images were taken as reference for an automatic linear spatial alignment (Automated Image Registration package; Woods et al., 1992) of the two dynamic acquisitions. Subsequently, the bihippocampal plane was defined on the mean image of the aligned dynamics to reslice acquisitions in hippocampal orientation. The same transformation matrix was applied to the dynamic data set. Similarly, transverse MR images were reoriented in the hippocampal plane coregistered with the mean PET by means of AIR (Woods et al., 1993) and resliced with same sampling as the PET data. This image preprocessing resulted in a complete data set (anatomic MR imaging, and dynamic PET) with common orientation and size.

After registering these MR imaging data, we drew 27 volumes of interest using a contour tool (CAPP; CTI-Siemens). For each region the time-activity mean curves were extracted and converted into time-concentration curves. Volumes of interest were drawn in the cerebellum, pons, in the left and right cortical regions (occipital, temporal, prefrontal, inferior parietal, anterior cingulum, insula, temporal pole, and entorhinal), in the left and right amygdala, hippocampus, parahippocam-pus, and in the raphe nuclei, longitudinal sinus, and in a intensely

labeled region in the posterior part of scalp. For the raphe nuclei, which are difficult to delineate on MR images, the contours were first drawn on the averaged PET image and then displayed on the subject's MR image to verify their proper location in the periaqueducal gray matter of the cerebral trunk. Volumes of interest ranged from 0.37 cm^3 for the raphe nuclei to 15 cm^3 for the volume of interest traced in the temporal neocortex.

Compartmental model and tracer kinetics analysis

A three-compartment model was applied to quantify the exchanges of MPPF between vascular networks, tissues, and 5-HT_{1A} receptors (Fig. 1; Appendix A).

From this model we applied two different approaches to estimate the 5-HT_{1A} receptor binding (Appendix B). We performed (1) a complete nonlinear (CNL) resolution of the model with the arterial blood sample as input function and regional PET kinetics, where the six unknown parameters (K_1, k_2, k_{on}/Vr, k_{off}, B_{max}, and F_v) were identified by minimization of a weighted least-square method (CNL method); and (2) a graphical projection of the kinetics based on the Logan-Patlak plot (Logan method; Delforge et al., 1995; Logan et al., 1990), which determines the total distribution volume (DV) in a region (V_t^L). The relations between solved parameters of the CNL method and graphically estimated parameters of the Logan method are established in Appendix C. From the parametric results of the CNL method, analytical values for V_2, V_3, V_t, BP, and $BP^L_{analytic}$ were computed and compared with the graphical values obtained from plot of the Logan method (V_t^L and BP^L). The differences in regional distribution of model parameters and indices were evaluated with an analysis of variance. A significant threshold was set at 0.001. A Bonferroni correction was applied in case of multiple comparisons of noninde-pendent data.

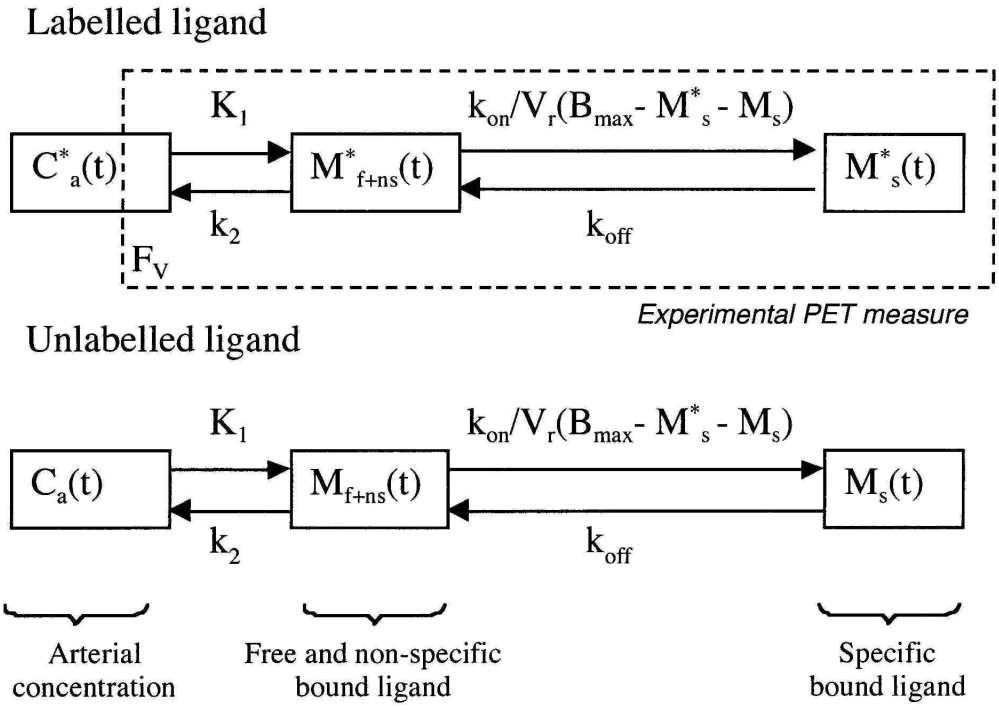

FIG. 1. *Three-compartment ligand-receptor model adapted from Delforge et al., (1990). Exchange rates are linear, except for the specific binding rate, which is related to the bimolecular association constant k_{on} and to the available receptor site concentration (B_{max} minus labeled and unlabeled specifically bound ligand). The positron emission tomography experimental measures are the sum of labeled ligand concentration in the free and nonspecific compartment, and in the specific compartment plus the F_v fraction of arterial concentration in labeled* MPPF.

Published in: Journal of cerebral blood flow and metabolism (2002), vol. 22, iss. 6, pp. 753-765
Status: Postprint (Author's version)

RESULTS

Arterial concentration

The analysis of arterial concentrations of [^{18}F]MPPF and its metabolites revealed a rapid metabolization of the ligand (Fig. 2); within 10 minutes, 86% of the arterial MPPF was converted to one principal polar metabolite as measured by high-pressure liquid chromatography. The experimental arterial function was reproducible between subjects and between injections. The percentage of metabolized [^{18}F]MPPF over time followed the equation $P_{metab}(t_{min} < 2) = 1$, and $P_{metab}(t_{min} > 2) = 1.79e^{-0.40\ t}+0.13e^{-0.03\ t}$ with a standard error fit of 8%.

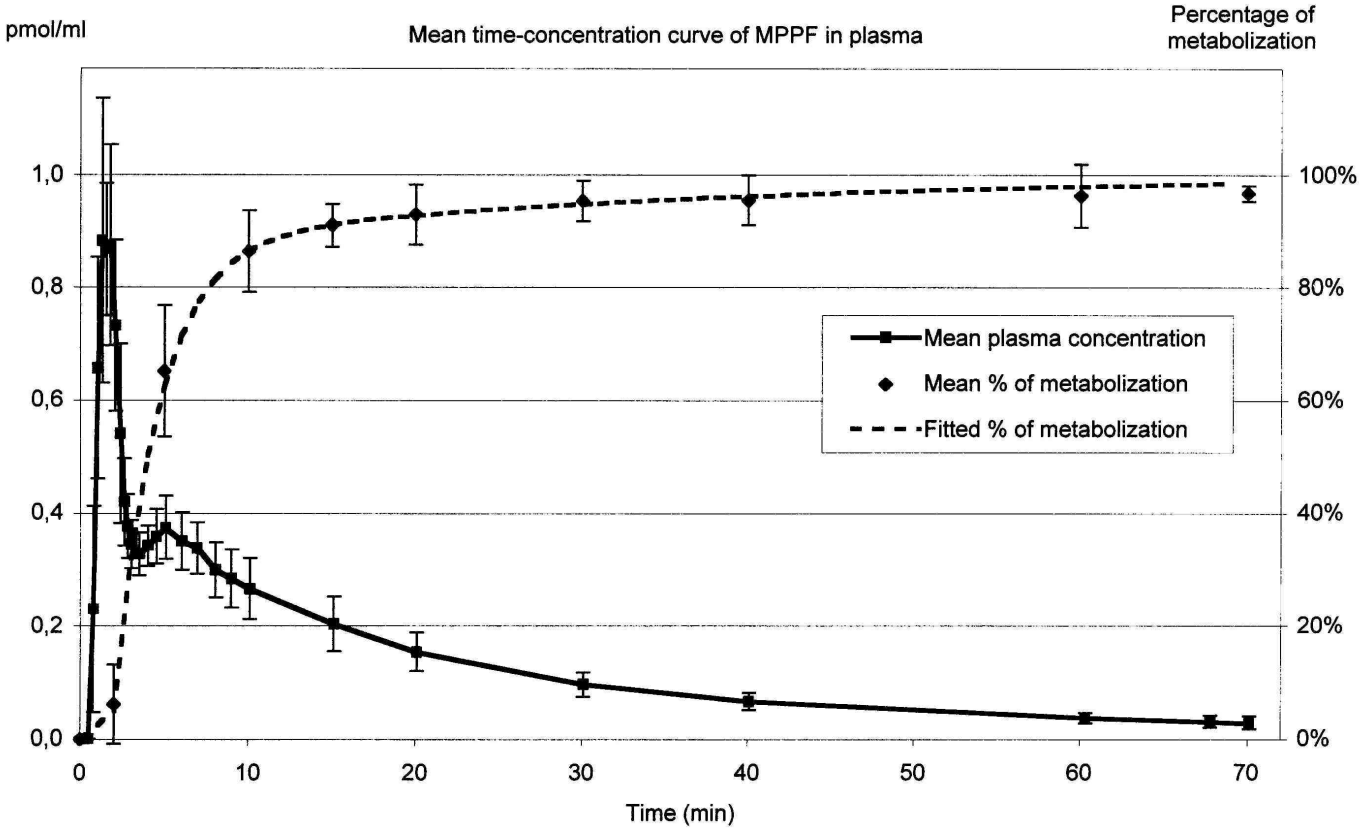

FIG. 2. *Left scale: time-concentration curve of the MPPF in plasma in pico-moles per milliliter. Right scale: percentage of metabolized [^{18}F]MPPF in plasma. Data are mean values ± SD for five subjects.*

Positron emission tomography images

The PET static images (sum of images between 20 and 70 minutes after injection) showed a high uptake of the tracer in the hippocampi, parahippocampal gyri, and amygdala, and a less intense concentration in neo-cortical regions. The radioactivity in cerebellum, pons, and striatum was largely under the mean. On the contrary, the concentration of the tracer was high in the veins, sagittal sinus and carotids, and in the posterior aspect of the scalp. Raphe nuclei were identified in the cerebral trunk, in a region apparently devoid of tracer accumulation (Fig. 3).

Positron emission tomography kinetics

Time-concentration curves revealed a rapid inflow and washout in the cerebellum and the pons. On the contrary, in target regions, the time-concentration curves were delayed by an apparent fixation. The late accumulation in the region of the scalp has a delayed kinetic. The time-activity curve in raphe nuclei was very noisy. The variance of these regions revealed that noise in the raphe was the same magnitude as that in other randomly tested cortical regions of similar size. Examples of individual kinetic curves are presented in Fig. 4.

Published in: Journal of cerebral blood flow and metabolism (2002), vol. 22, iss. 6, pp. 753-765
Status: Postprint (Author's version)

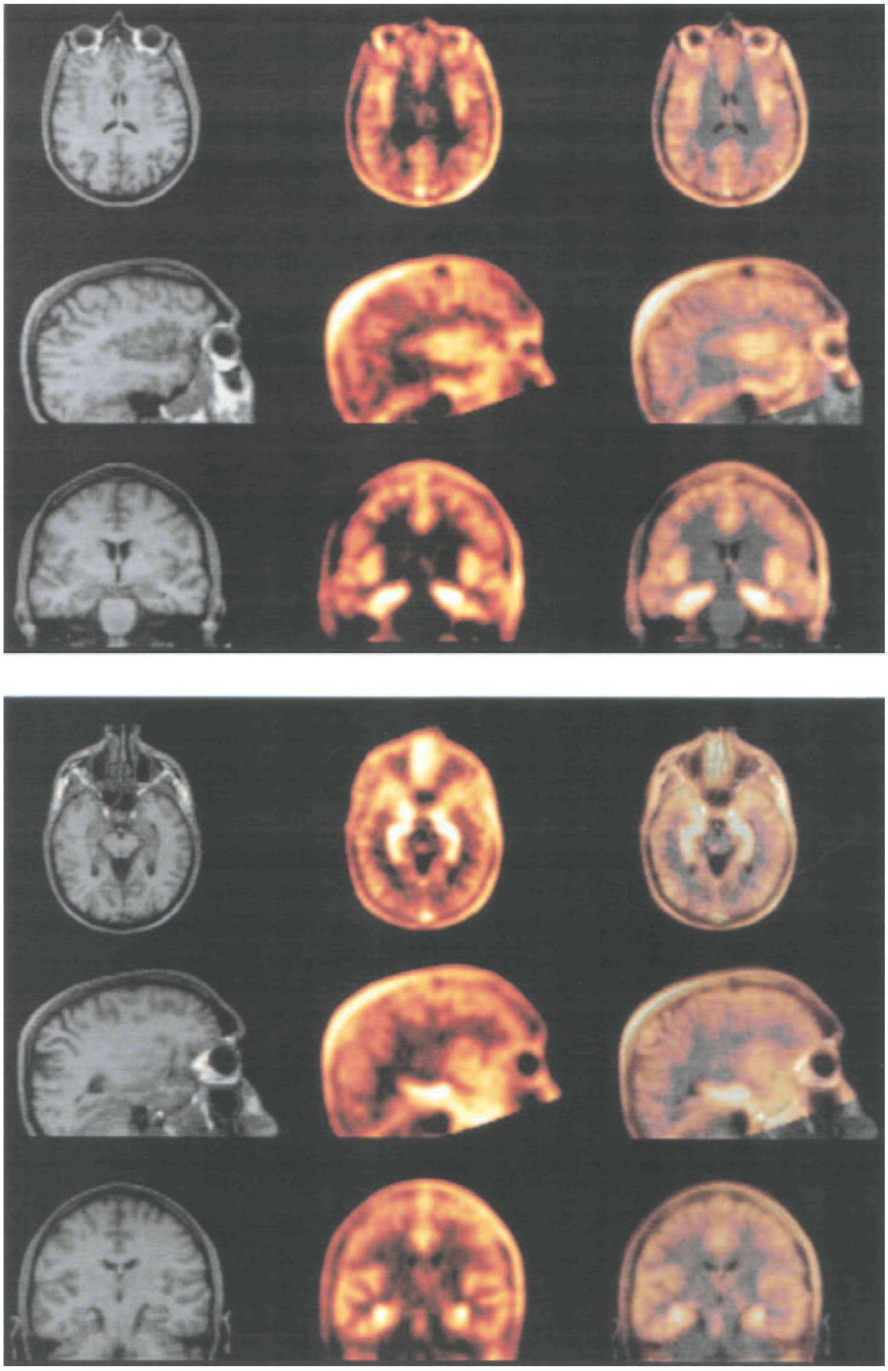

FIG. 3. *Images of anatomical magnetic resonance (MR) images and [^{18}F]MPPF positron emission tomography (PET). Top: view of the insula. Bottom: view of the hippocampic and raphe nuclei binding. MR (left row), [^{18}F]MPPF PET (middle row), and fusion (right row) images for subject 1.*

Published in: Journal of cerebral blood flow and metabolism (2002), vol. 22, iss. 6, pp. 753-765
Status: Postprint (Author's version)

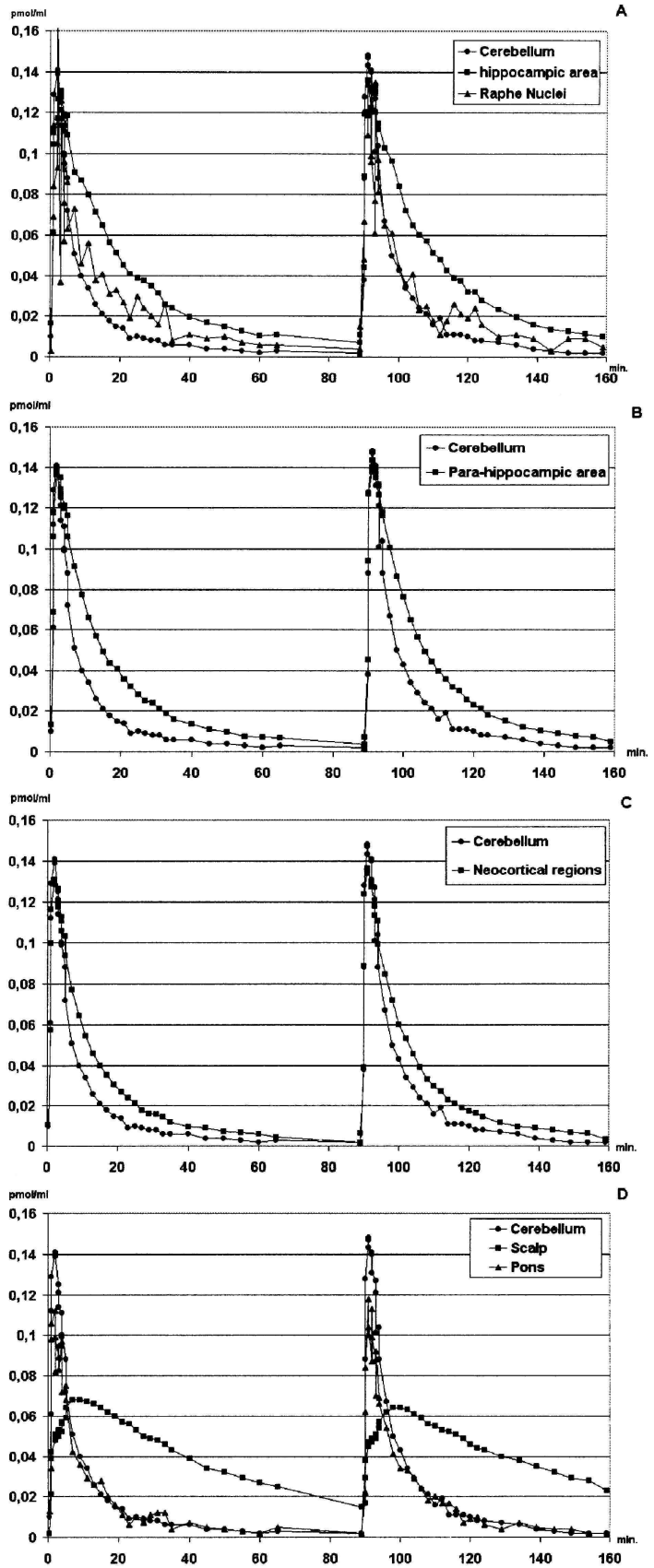

FIG. 4. *Typical time-concentration curves in one subject after bolus injection at time zero and at time 89 minutes. Plots are corrected for decay of radioactivity. (A) Mean of hippocampal areas and raphe nuclei. (B) Mean of parahippocampal area. (C) Mean of neocortical regions. (D) Scalp and pons. Left and right curves are averaged, and in each plot the cerebellum is plotted for reference.*

Model parameter estimation

Table 2 reports the estimation of the model parameters after fitting for the right hippocampus region and the right prefrontal cortex. Table 3 describes the average over five subjects of the model parameters after fitting.

To assess the interregional variability, we grouped regions in four categories: (1) the *limbic areas* (hippocampus and amygdala), (2) the *paralimbic area* (parahippo-campal gyrus, entorhinal cortex, insula, cingulum, and temporal pole), (3) the *neocortical regions* (temporal, occipital, parietal, and prefrontal neocortex), and (4) *other regions* (cerebellum and pons).

Blood-brain barrier rate. The relative error of fit for the K_1 and k_2 parameters was small (2% to 6% error for K_1 , and 4% to 10% for k_2). K_1 was close to 0.100/min in limbic regions, superior to 0.110/min in neocortical areas, and approximately 0.095 in the cerebellum. A SD and a relative difference close to 20% were found between subjects. In the pons, the influx rate in the tissue compartment was smaller, with a value of 0.047/min. The k_2 values were regrouped the same way, and ranged from 0.135/min to 0.179/min in limbic regions, and from 0.220/min to 0.270/min in neocortical regions and in the pons. The value in temporal poles was intermediate (k_2 = 0.180/min). Finally, the cerebellum showed the biggest washout, with a k_2 of 0.302/min.

Vascular fraction. The vascular fraction (F_v) was close to the standard value of 0.04 (the mean over regions and subjects was 0.041 ± 0.023). The blood-tissue partition was much higher in the cerebellum and in the pons, with values of 0.08 and 0.06, respectively. A variance analysis of F_v revealed that the differences between pons and cerebellum and all the other regions was significant *(*$P < 0.0002$), whereas the F_v values between limbic, paralimbic, and neocortical regions was not significant.

Binding parameters. The average density of 5-HT_{1A} receptors ranged from 1.5 to 1.8 pmol/mL in the occipital, temporal, prefrontal, and parietal cortices. Densities ranged from 1.5 to 2.3 in the paralimbic regions group, with the lowest value in the anterior cingulate cortex. In limbic regions, the mean density ranged from 1.9 pmol/mL in the amygdala to 2.9 pmol/mL in the hippocampus. This density was significantly different in limbic areas and in neocortical regions *(*$P < 0.018$, Bon-ferroni corrected). The temporal pole density was 2 pmol/mL. Among all regions, there was no significant difference between left and right values *(*$P > 0.17$), and left and right results are averaged in Tables 3 and 4. A mean receptor density of 1.77 pmol/mL (0.59 SD for a mean over the five subjects) was calculated for the raphe nuclei. We failed to identify a value of receptor density in the cerebellum and the pons using the three-compartment model because the standard error for B_{max} exceeded the tolerance threshold. Therefore, we had to test two different models: a first model considering two compartments, and another introducing a third compartment to test for specific or nonspecific binding (Table 3). For the cerebellum, the best fit was found for the three-compartment model, whereas for the pons there was no significant difference in quality of fit between the two-compartment and three-compartment models.

Dissociation rate. The ratio between k_{off} and k_{on}/V_r was relatively constant over the regions. The mean value was 0.023/min ± 0.016/min for k_{on}/V_r, and 0.047/min ± 0.015/min for k_{off}. All regional values for these parameters were included in the mean ± 2 SD range. No significant difference was found between regions or between groups of regions. Consequently, the apparent dissociation constant (K_d) was stable over regions, with a mean value of 2.8 ± 1.41 nmol/L.

Simplified method correlation

Analytical values of DVs and binding potential (BP) were computed from the model parameters and averaged over subjects on the data set of 23 regions (Eqs. 2, 3, 4, 5, and 6 in Appendix C). From the Logan-Patlak graphic, we evaluated the asymptote slope (V_t^L) and computed the binding potential (BP^L; Eq. 1, Appendix B) using the cerebellum V_t^L as tissue reference. Results are reported in Table 4.

Distribution volume. The analytical nonspecific and free DV (V_2, Eq. 2) had a mean value of 0.53 ± 0.08. The highest values were found in paralimbic regions (0.59 ± 0.14), then in limbic areas (0.55 ± 0.09) and in neocortical regions (0.48 ± 0.10). The lowest values were calculated in the cerebellum (0.33 ± 0.1). A variance analysis performed on V_2 using region groups as a factor showed a significant regional variability *(*$P < 0.0001$). A *post hoc* analysis also revealed a significant difference between (1) the cerebellum and the other region groups *(*$P < 0.0001$) and (2) neocortical regions and paralimbic regions *(*$P < 0.0001$), but no significant difference between (3) paralimbic and limbic regions and (4) limbic and neocortical regions. The DV issued from the Logan method (V_t^L) ranged from 1.02 in cerebellum to 2.3 in hippocampus. The linear regression analysis of DVs computed on compartmental model parameters V_t versus V_t^L, was significant: $V_t^L = 1.60\ V_t + 0.43$ *(*R^2 =

0.86, $P < 0.001$).

Binding potential. Analytical values of BP (Eq. 5) ranged from 0.43 in the cerebellum to 1.18 in the hippocampus, with approximate values of 1.0 in other limbic regions, 0.7 in the entorhinal cortex and amygdala, and 0.55 in neocortical regions. The temporal pole reached a value of 0.8. The analytical value V_3 (Eq. 3) was distributed the same way as BP over regions, but with a lower magnitude. The BP evaluated with the graphical analysis of the Logan method (BP^L), using cerebellum DVs as reference, ranged from 0 (reference) to 1.3 in the hippocampus. In particular, BP^L values were approximately 1.0 in paralimbic regions (except in entorhinal cortex, 0.8), and between 0.6 and 0.7 in other cortical regions, whereas the lowest value was found in the occipital cortex (0.37).

A correlation analysis was performed to compare the distribution of BP^L with analytical indices computed with the compartment model. These results are presented in Figure 5. The BP^L was strongly correlated with BP^Lanalytic ($R^2 = 0.88$, $P < 0.001$). Significant correlations were found with V_3, V_t, and B_{max} . Plots of BP^L versus compartmental BP were more scattered and correlation was at the limit of significance ($P = 0.011$). K_d was not linearly correlated to BP^L.

TABLE 2. *Values of the model parameters estimated on five subjects with nonlinear fitting method in two typical regions*

ROIs	B_{max} (pmol/mL ± SD)	K_1 (min^{-1} ± SD)	k_2 (min^{-1} ± SD)	k_{0n}/V_r ($ml \cdot pmol^{-1} \cdot min^{-1}$ ± SD)	k_{off} (min^{-1} ± SD)	F_v (ml/pmol ± SD)	$K_D V_r$ (nmol/L ± SD)
Right hippocampus							
Subject							
1	3.510 ± 1.355	0.115 ±0.004	0.169 ±0.010	0.013 ± 0.005	0.040 ± 0.002	0.020 ± 0.009	3.063 ± 1.363
2	2.864 ± 0.856	0.096 ± 0.004	0.173 ±0.011	0.011 ±0.003	0.038 ± 0.002	0.034 ± 0.006	3.410 ± 1.217
3	4.813 ±0.585	0.155 ±0.004	0.218 ±0.008	0.010 ±0.001	0.041 ± 0.002	0.077 ±0.011	4.079 ± 0.664
4	0.812 ±0.330	0.064 ± 0.004	0.129 ±0.014	0.046 ±0.018	0.042 ± 0.005	0.034 ± 0.009	0.916 ±0.464
5	2.340 ± 1.907	0.083 ± 0.005	0.182 ±0.021	0.019 ±0.016	0.043 ± 0.004	0.018 ±0.009	2.257 ± 2.068
Right prefrontal							
Subject							
1	2.653 ± 1.782	0.175 ±0.004	0.334 ±0.016	0.021 ± 0.015	0.077 ± 0.009	0.033 ± 0.006	3.624 ± 2.932
2	2.340 ± 1.441	0.107 ±0.004	0.232 ±0.011	0.005 ± 0.003	0.022 ± 0.003	0.031 ±0.007	4.179 ±2.935
3	2.564 ± 0.433	0.186 ±0.008	0.334 ± 0.022	0.015 ± 0.003	0.053 ± 0.007	0.055 ± 0.014	3.493 ± 1.091
4	0.429 ±0.183	0.091 ± 0.005	0.212 ±0.013	0.054 ± 0.024	0.043 ± 0.004	0.035 ± 0.010	0.809 ± 0.438
5	0.425 ±0.171	0.095 ± 0.004	0.243 ± 0.012	0.047 ±0.019	0.038 ± 0.003	0.035 ± 0.007	0.805 ± 0.394

SD is the estimated standard deviation resulting from the fit procedure, calculated with the covariance matrix.

Published in: Journal of cerebral blood flow and metabolism (2002), vol. 22, iss. 6, pp. 753-765
Status: Postprint (Author's version)

TABLE 3. *Mean values (left/right averaged) of the model parameters estimated on five subjects with nonlinear fitting method*

ROIs	B_{max} (pmol/ml ± SD)	k_1 (min^{-1} ± SD)	k_2 (min^{-1} ± SD)	k_{on}/V_r (ml· $pmol^{-1}$ · min^{-1} ± SD)	k_{off} (min^{-1} ± SD)	F_v (ml/pmol ± SD)	K_DV_r (nM ± SD)
Limbic areas							
Hippocampus	2.778 ±1.384	0.103 ±0.033	0.176 ±0.036	0.020 ±0.012	0.040 ± 0.003	0.036 ±0.022	2.575 ±1.040
Amygdala	1.962 ±1.038	0.089 ±0.028	0.169 ±0.041	0.018 ±0.005	0.042 ± 0.015	0.052 ± 0.023	2.475 ±0.861
Limbic average	2.370 ±1.262	0.096 ±0.031	0.173 ±0.038	0.019 ±0.009	0.041 ±0.011	0.044 ± 0.023	2.525 ±0.931
Paralimbic areas							
Parahippocampal gyrus	2.343 ±1.136	0.099 ±0.028	0.159 ±0.031	0.016 ±0.011	0.042 ± 0.007	0.040 ± 0.029	3.319 ±1.312
Enthorinal cortex	2.034 ±1.131	0.097 ± 0.026	0.141 ±0.012	0.020 ±0.015	0.043 ±0.011	0.028 ±0.023	2.943 ±1.447
Temporal pole	1.961 ±1.157	0.102 ±0.035	0.184 ±0.032	0.027 ±0.017	0.047 ± 0.013	0.031 ±0.014	2.417 ±1.265
Insula	1.984 ±1.225	0.126 ±0.043	0.222 ± 0.048	0.022 ±0.015	0.051 ± 0.004	0.053 ±0.016	3.413 ±1.890
Anterior Cingulum	1.504 ±1.093	0.128 ±0.042	0.239 ± 0.069	0.023 ±0.012	0.059 ± 0.036	0.052 ±0.021	2.905 ±1.268
Posterior Cingulum	1.670 ±0.963	0.145 ±0.049	0.275 ± 0.065	0.022 ±0.012	0.056 ± 0.027	0.051 ±0.016	3.252 ±1.696
Paralimbic average	1.982 ±1.108	0.112 ±0.038	0.193 ±0.059	0.021 ±0.014	0.048 ±0.016	0.040 ± 0.022	3.304 ±1.466
Neocortical regions							
Temporal neocortex	1.612 ±1.170	0.118 ±0.032	0.217 ±0.027	0.030 ±0.027	0.048 ± 0.009	0.032 ±0.016	2.851 ±1.766
Occipital cortex	1.512 ±0.821	0.118 ±0.041	0.278 ± 0.039	0.026 ±0.018	0.047 ± 0.006	0.024 ±0.010	2.637 ±1.380
Parietal cortex	1.721 ±1.189	0.134 ±0.043	0.269 ± 0.052	0.026 ±0.017	0.051 ± 0.022	0.037 ±0.012	2.710 ±1.465
Prefrontal cortex	1.702 ±1.056	0.133 ±0.043	0.278 ± 0.057	0.030 ±0.020	0.052 ± 0.022	0.036 ±0.009	2.651 ±1.653
Neocortical average	1.637 ±1.031	0.126 ±0.039	0.260 ± 0.051	0.028 ±0.020	0.049 ± 0.016	0.032 ±0.013	2.712 ±1.514
Other areas							
Pons (2 comp)		0.047 ±0.015	0.219 ±0.074			0.064 ±0.014	
Pons (3 comp)		0.070 ± 0.026	0.298 ± 0.034	0.016$± 0.012	0.039* ±0.025	0.047 ± 0.032	
Cerebellum (2 comp)		0.095 ± 0.040	0.302 ± 0.069			0.085 ±0.037	

Published in: Journal of cerebral blood flow and metabolism (2002), vol. 22, iss. 6, pp. 753-765
Status: Postprint (Author's version)

Cerebellum (3 comp)	0.152 ±0.055	0.459 ± 0.052	0.022$± 0.006	0.050* ±0.009	0.014 ± 0.011
Other areas average (3 comp)	0.116 ±0.060	0.387 ± 0.095	0.019$± 0.009	0.045* ±0.018	0.028 ±0.027

SD is the standard deviation from the 5 subjects. * These values have to be taken as k_4 for k_{off}. $ These values have to be taken as k_3 for k_{on} B_{max}.

Published in: Journal of cerebral blood flow and metabolism (2002), vol. 22, iss. 6, pp. 753-765
Status: Postprint (Author's version)

TABLE 4. *Indices derived from the multicompartmental model and the Logan methods*

Regions	v_2	v_3	**BP**	v_t	$V_{t\ target} / V_{t\ reference} - 1$	V_t^L	BP^L
Limbic areas							
Hippocampus	0.58 ±0.10	0.61 ±0.19	1.04 ±0.17	1.18 ±0.28	1.54 ±0.19	2.33 ±0.16	1.33
Amygdala	0.52 ± 0.08	0.39 ±0.14	0.75 ± 0.22	0.92 ± 0.20	0.97 ±0.16	1.93 ± 0.21	0.93
Limbic areas average	0.55 ± 0.09	0.50 ±0.19	0.90 ± 0.24	1.05 ± 0.28	1.26 ± 0.34	2.13 ± 0.27	1.13
Paralimbic areas							
Parahippocampal gyrus	0.63 ±0.16	0.43 ±0.16	0.68 ±0.14	1.06 ± 0.30	1.27 ± 0.29	2.20 ± 0.26	1.20
Entorhinal cortex	0.69 ±0.19	0.48 ±0.17	0.69 ±0.10	1.18 ±0.36	1.49 ± 0.21	2.14 ±0.20	1.14
Insula	0.56 ±0.11	0.32 ±0.12	0.56 ±0.13	0.88 ± 0.21	0.88 ±0.14	2.09 ± 0.32	1.09
Cingulum	0.53 ± 0.08	0.26 ±0.11	0.49 ±0.18	0.79 ±0.17	0.70 ±0.14	1.78 ±0.11	0.78
Temporal pole	0.54 ±0.11	0.45 ± 0.22	0.80 ± 0.25	0.99 ±0.31	1.10 ±0.20	1.95 ±0.19	0.95
Temporal cortex	0.54 ±0.12	0.30 ±0.10	0.54 ± 0.09	0.84 ± 0.21	0.80 ±0.13	1.75 ±0.09	0.75
Paralimbic areas average	0.59 ±0.14	0.39 ±0.17	0.64 ±0.19	0.98 ± 0.30	1.09 ± 0.34	2.03 ± 0.26	1.03
Neocortical regions							
Occipital cortex	0.42 ±0.10	0.24 ± 0.08	0.58 ± 0.09	0.66 ±0.17	0.41 ± 0.09	1.37 ±0.08	0.37
Parietal cortex	0.49 ± 0.09	0.30 ±0.13	0.59 ±0.16	0.78 ± 0.21	0.68 ±0.18	1.68 ±0.14	0.68
Frontal cortex	0.47 ± 0.07	0.30 ±0.10	0.62 ±0.13	0.77 ±0.16	0.67 ±0.14	1.66 ±0.09	0.66
Temporal pole	0.54 ±0.11	0.45 ± 0.22	0.80 ± 0.25	0.99 ±0.31	1.10 ±0.20	1.95 ±0.19	0.95
Neocortical regions average	0.48 ±0.10	0.28 ±0.10	0.58 ±0.12	0.76 ±0.19	0.64 ± 0.20	1.62 ±0.18	0.62
Other areas							
Pons (3 comp)	0.23 ± 0.07	0.09 ± 0.04	0.38 ± 0.06	0.32 ±0.10	-0.41 ±0.19	—	—
Pons (2 comp)	0.22 ± 0.08					—	—
Cerebellum (3 comp)	0.33 ±0.15	0.14 ±0.30	0.43 ± 0.35	0.47 ± 0.45	0.00	—	—
Cerebellum (2 comp)	0.31 ±0.09					—	—

V_2, distribution volume in the free and nonspecific compartment (Appendix C, Eq. 2); V_3, distribution volume in the specific binding compartment (Appendix C, Eq. 3); BP, binding potential (Appendix C, Eq. 5); V_t, total distribution volume (Appendix C, Eq. 4); $V_{t\ target}/V_{t\ reference}-1$, analytic value of Logan binding potential (Appendix C, Eq. 6); V_t^L, total distribution volume from Logan method; BP^L, binding potential from Logan method. (SD on 5 subjects.)

Published in: Journal of cerebral blood flow and metabolism (2002), vol. 22, iss. 6, pp. 753-765
Status: Postprint (Author's version)

DISCUSSION

The aim of this study was to quantify the *in vivo* exchange of MPPF with the serotonergic 5-HT_{1A} receptors using a compartmental model. An experimental design was defined to achieve the determination of six unknown parameters characterizing the model. The resolution of the system provided a complete quantitative overview of the exchange rates, the density of 5-HT_{1A} receptors, and the affinity of MPPF for receptors over 24 anatomical brain regions.

MPPF distribution in blood and brain

Our data regarding arterial function are concordant with the results of previous [^{18}F]MPPF studies (Pass-chier et al., 2000*a,b),* which reported, in two different groups of subjects, that 10% of the original ligand was present in plasma 10 minutes after injection. The me-tabolization reported in the present study is slightly slower. On average, we found that 14% of unmodified ROI, region of interest; B_{max}, concentration of available receptor sites; $K_{1;}$ entrance blood-to-brain transfer rate; k_2, escape blood-to-brain transfer rate; k_{on}/V_r, bimolecular association constant relative to volume of reaction; k_{off}, bimolecular dissociation constant; F_v, vascular fraction; K_DV_r, equilibrium dissociation constant.

ROI, regions of interest; B_{max}, concentration of available receptor sites; K_1, entrance blood-to-brain transfer rate; k_2 escape blood-to-brain transfer rate; k_{on}/V_r, bimolecular association constant relative to volume of reaction; k_{off}, bimolecular dissociation constant; F_v, vascular fraction; K_DV_r, equilibrium dissociation constant.

MPPF was present 10 minutes after injection. The dispersion of individual curves was not significant, and the use of a standard biexponential equation for metabolite correction of blood samples might be considered a good approximation.

In agreement with findings of previous [^{18}F]MPPF-PET studies (Passchier et al., 2000*a,b;* Passchier et al., 2001), equilibrium static images showed a high tracer uptake in limbic areas and in paralimbic regions. Compared with other limbic and paralimbic areas, cingulum and entorhinal cortices showed less tracer accumulation. The values in these latter regions were more similar to those found in neocortical areas. This particular distribution within paralimbic areas has not been observed with WAY 100635 images (Gunn et al, 1998). However, a direct comparison of raw data between different tracers should be viewed with caution because multiple parameters are involved. Thus, receptor density parametric images should be computed to ensure reliable comparisons. This, however, was outside the scope of our study.

Raphe nuclei were clearly discernable, and the coreg-istration with MR imaging data allowed us to confirm their anatomical localization in the cerebral trunk, dorsal to the periaqueductal gray matter. In all of our subjects, raphe nuclei were detected on several transverse planes (typically two to five planes, which corresponds to 5 to 12 mm). The extension of this structure in the vertical direction is not well adapted to the transverse acquisition plane imposed by the PET scanner. Moreover, the size of the apparent structure on PET images exceeded the actual size of the anatomic structure, which indicates that a partial volume effect altered the measure. A volumetric three-dimensional correction would be necessary to evaluate the real concentration of tracer in such small structures. This work is currently in progress.

Model parameter identification

Identification of model parameters was possible and relatively accurate despite the low difference between apparent specific activities that were chosen for injections. Theoretically, the optimal protocol for parameter estimation of a multicompartmental model includes a first injection at the tracer dose, a displacement with the unlabeled ligand, and a coinjection of labeled and unlabeled ligands to saturate the receptor sites (Delforge et al., 1989; Delforge et al., 1990). Using such a protocol, the resolution of the equation system leads to a unique solution. However, in our case a displacement injection would have implied a massive injection of unlabeled MPPF. Because behavioral effects of a large dose of MPPF have not been tested in humans, we limited, for pharmacologic safety reasons, the amount of coinjected unlabeled MPPF to achieve a tenfold-lower specific activity for the second injection. Therefore, in our protocol, the resolution of the equation system might lead to a nonunique solution. The reliability of the solution has to be tested, possibly using two different techniques. First, the definition of constraints regarding some of the parameters allows the achievement of pharmacologically realistic solutions. For example, we excluded mathematical solutions for which the K_d value exceeded an interval of ± 10 times the *in vitro* value of K_i (3.3 nmol/L; Zhuang et al., 1994). The use of such constraints usually leads to a solution in which the value of the parameters fell within an acceptable SD. Second, the stability of the

solution can be tested to rule out local minima. To test the stability, we changed the initial values defined before the fit procedure and checked that the algorithm converged toward the same final parameters. The distribution of receptor density in target regions reflected the visual inspection of raw static images. To assess the validity of our results, we plotted the distribution of receptor density measured by PET with [^{18}F]MPPF against results of autoradiographic binding on resected human tissues with [^{3}H]WAY-100635 (Burnet et al., 1997; Hall et al., 1997). Despite the disproportion of absolute values for the density between *ex vivo* radiographic data and *in vivo* PET measurements, we found an excellent correlation between these two approaches (see Figure 6). Regarding the density of 5-HT_{1A} receptors in the cingulate cortex, the B_{max} for this region closely matched that of other neocortical regions. This profile was also observed in the study of Hall et al. (1997), whereas Burnet et al. (1997) found a ratio of 1.5 between the cingulum and temporal cortex. Concerning the raphe nuclei, our modeling provided a value for the density of 5-HT_{1A}. However, the statistical noise for these data and the partial volume effect due to the small size (close to the resolution) of the structure gave a relative poor value of B_{max} and a high uncertainty regarding the quality of fit because the relative error was two or three times larger than the parameter value itself. For these reasons, these results were not reported in Table 3.

Because a pharmacologic displacement with unlabeled MPPF was not possible in this study, the free and nonspecific compartments could not be assessed individually. Therefore, in regions for which the identification of three compartments was not possible, we considered only two compartments (i.e., a vascular compartment and a single tissular compartment). However, in this case, we introduced an auxiliary compartment to test for the binding of ligand in the cerebellum and pons with no separate identification of B_{max} and k_{on} ($k_3 = k_{on}B_{max}$). For the cerebellum, the two-compartment model (a common compartment for free and nonspecific binding) provided K_1 and k_2 values of 0.095/min and 0.302/min, respectively. Besides in the three-compartment model, values for K_1 and k_2 were 0.152 and 0.459, and values for k_3 and k_4 were 0.022/min and 0.050/min. We could verify that $k_2/(1 + k_3/k_4)$ equals 0.318, which was close to the apparent k_2 found in the two-compartment model. Because the dissociation rate found for this supplementary compartment in cerebellum (k_4) was close to the mean dissociation rate of target region ($k_{off} = 0.047$), and because the fit was better if we considered three rather than two compartments, we assumed that this auxiliary compartment, because of its kinetic parameters, represented a specific association to 5-HT_{1A} receptor. Because metabolites are polar and do not cross the brain-blood barrier, this interpretation suggests that 5-HT_{1A} receptors may be present in the cerebellum, but with such a small density that our method cannot dissociate B_{max} and k_{on}/V_r. The same analysis (two-compartment and three-compartment separate fit) performed in the pons gave values of 0.047 and 0.219 for K_1 and k_2, and 0.070, 0.298, 0.016, and 0.039 for K_1, k_2, k_3 and k_4, respectively. Once again, the $k_2/(1 + k_3/k_4)$ ratio equals 0.211/min, which was close to the k_2' value computed by the two-compartment model. In this case, k_4 was significantly different from the mean k_{off}, suggesting no specific binding in the pons.

Published in: Journal of cerebral blood flow and metabolism (2002), vol. 22, iss. 6, pp. 753-765
Status: Postprint (Author's version)

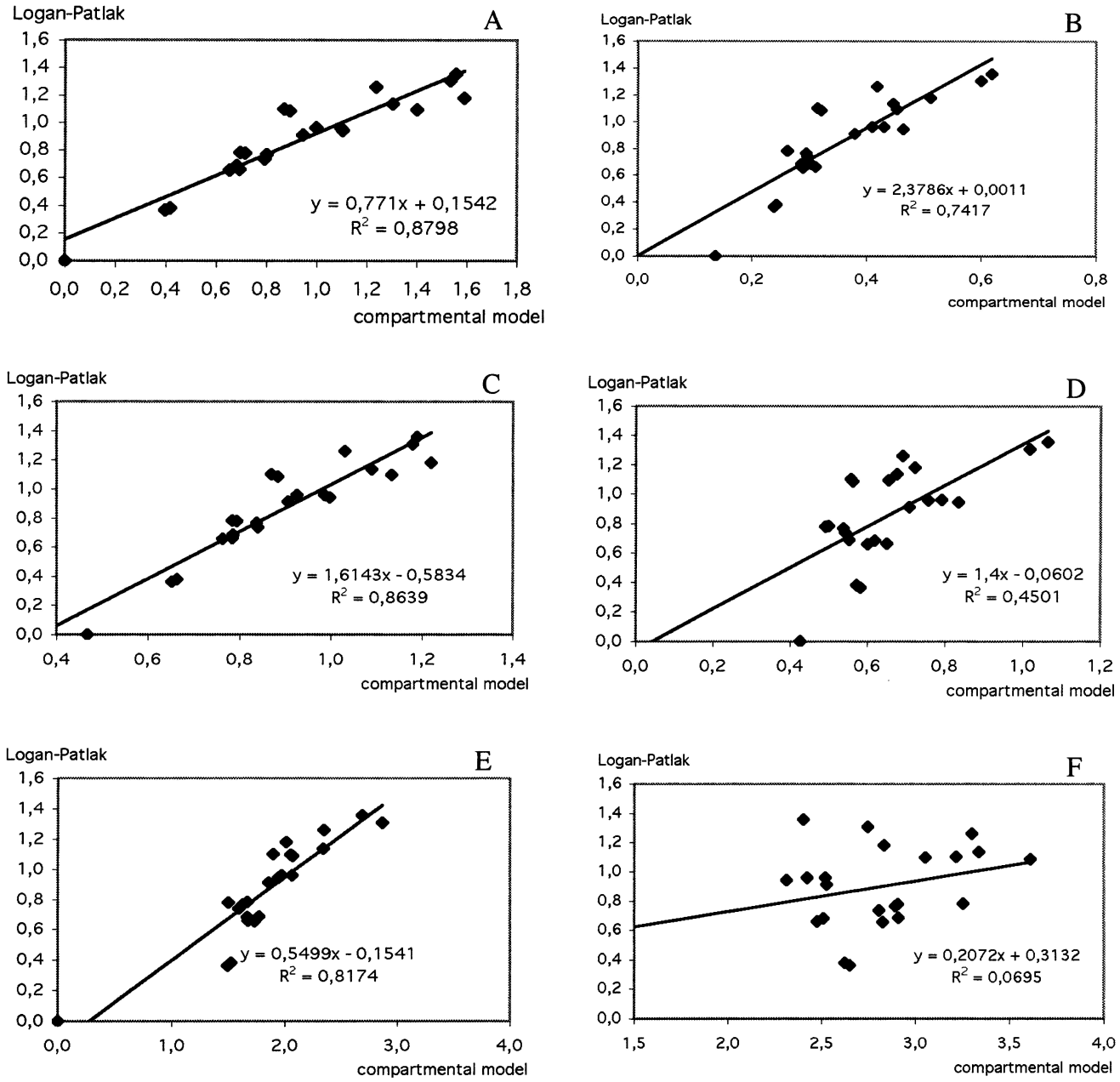

***FIG. 5**. Correlation between binding potential (BP) measured by Logan graphical method (BP^L) with a reference tissue input function, and analytical values of distribution volumes (DVs) and binding potential computed from the compartmental model parameters (Appendix C). (A) BP^L versus ratio of total DV in the target and reference regions minus one ($BP^L_{analytic}$ Eq. 6). (B) BP^L versus DV in the specific compartment (V_3, Eq. 3). (C) BP^L versus total DV (V_t, Eq. 4). (D) BP^L versus BP from the nonlinear method (BP, Eq. 5). (E) BP^L versus density of receptors (B_{max}). (F) BP^L versus the apparent equilibrium dissociation constant (K_d).*

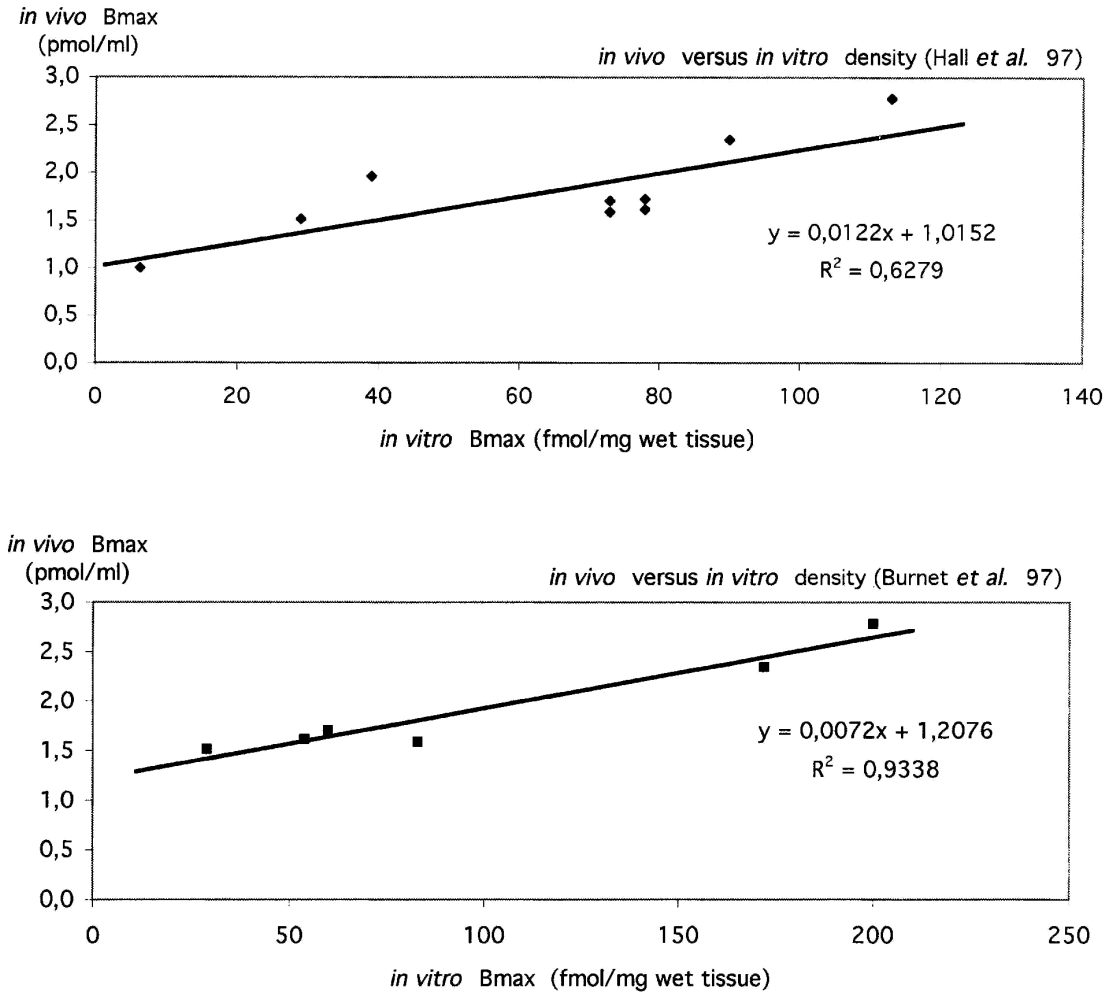

FIG. 6. *Correlation between the density measured in vitro by [^{3}H]WAY-100635 autoradiography (Burnet et al., 1997; Hall et al., 1997) and measured in vivo by [^{18}F]MPPF positron emission tomography.*

Simplified reference tissue model

Using knowledge of the local exchange parameters, we were able to analytically compute classical indexes usually used in the quantification of PET images without arterial blood function. The analysis over all cerebral regions revealed that the DV was fairly constant in the limbic, paralimbic, and neocortical regions. We showed that the cerebellum has a different DV (considering two or three compartments). In the simplified method, which needs a reference tissue to compute a BP, one of the underlying hypotheses is that target and reference regions have an equivalent DV. This hypothesis was not confirmed in our study because we found different DV values in the cerebellum and in target regions.

Consequently, the cerebellum, known to have a poor concentration of 5-HT_{1A} receptors, should not be taken as a reference region for the evaluation of B_{max}/K_d without any correction. The correlation of the BP, computed from the graphical Logan method (BP^L), and analytic parameters issued from the CNL method, confirms this inadequacy (Fig. 5): there is poor linear correlation between the BP^L and BP (CNL method). This point suggests that the index measured by Logan method is not strictly linked to B_{max} and K_d. However, we found that Logan BP^L was closer to V_3, the BP multiplied by the DV of the nonspecific nondisplaceable compartment ($V_3 = V_2 \cdot B_{max}$). Furthermore, we verified that the analytic formula $V_{t\ target}/V_{t\ reference}^{-1}$ (Eq. 6) computed with model parameters was well correlated with BP^L. This finding confirms that the Logan method provides a good estimation of regional DV $V_{t\ target}$ and $V_{t\ reference}$. An interesting finding of this analysis was that BP^L was well correlated with B_{max}. This finding can be explained by the fact that even if K_d and k_2 are stable over regions, the ratio V_2/K_d also stays relatively constant over regions. This hypothesis was statistically verified by unpaired *t*-test on V_2/K_d. It can thus be concluded that even if BP^L was not a good index of B_{max}/K_d, it was nevertheless a

reliable index of receptor density in healthy subjects. Further investigations should assess if another region than cerebellum may provide a better reference for the quantification of receptor density.

CONCLUSIONS

A double-injection protocol was performed on healthy subjects to quantify the parameters of a compartmental model describing *in vivo* brain distribution of MPPF with PET. Compared with previously published results of *ex vivo* tissular receptor concentration, our results confirm the specificity of MPPF for 5-HT_{1A} receptors. A measurement of regional affinity indicates a mean *in vivo* $K_d.V_r$ value of 2.8 nmol/L for MPPF, which suggests that this ligand is a good candidate for determining the *in vivo* concentration variations for endogenous serotonin. Moreover this study confirms that, in the absence of blood arterial sampling, the BP estimated by the Logan method is a good index of local receptor concentration in healthy subjects, which allows for the calculation of MPPF parametric images.

APPENDIX A

Compartmental model

A three-compartment model was applied to quantify the exchanges of MPPF between vascular networks, tissues, and 5-HT_{1A} receptors (Fig. 1; Delforge et al., 1995). The first compartment, the *circulating plasma of the arterial network,* was represented in the model by the concentration $C_a(t)$ (in picomoles per milliliter plasma) of unmetabolized MPPF in the plasma. The second and third compartments were (1) the *free or nonspecific* compartment, represented by the quantity $M_{f+ns}(t)$, quantifying the free or nonspecifically bound ligand in 1 mL tissue; and (2) the *specific* compartment, represented by $M_s(t)$, quantifying the MPPF molecules specifically bound to the 5-HT_{1A} receptors in 1 mL tissue at time t. The assumption that the free and nonspecific compartment can be modeled by a single compartment is supported by the fact that exchanges between compartments are rapidly established (Plenevaux et al., 2000*b*). Moreover, displacement studies in rats revealed that proportion of nonspecific binding is negligible (Ginovart et al., 2000). Exchanges between compartments were defined by transfer rates. The value K_1 represented the inflow rate of ligand from plasma compartment to the free and nonspecific compartment, whereas k_2 was the escape rate from tissues to blood circulation. Exchanges between the free and nonspecific and the specific compartments were regulated by k_{on} for the bimolecular association rate, and k_{off} for the dissociation rate. These values depended on the quantity of available receptor sites B_{max} (i.e., the local density of receptors minus M_s, the actual occupied sites). In the regions where the density of available receptor is poor, B_{max} and k_{on} cannot be separately estimated. In this case, the model was first simplified to two compartments, where the rate k_2 was replaced by k_2'. Terms to be identified were then reduced to F_v, k_2' and k_1. Second, an identification of three compartments were tried, but with no separate estimation of B_{max} and k_{on} : these parameters were replaced by a unique rate $k_3 = k_{on}.B_{max}/V_r$ and k_{off} was replaced by k_4. The best fit was kept and we checked that the relation $k'_2 = k_2(1 + k_3/k_4)$ was verified.

Because of tissue heterogeneities, it was necessary to introduce the concept of volume of reaction, V_r (Del-forge et al., 1996). Because V_r is not discernable from k_{on}, only the ratio k_{on}/V_r can be estimated. The consequence is that the equilibrium dissociation rate K_d, which is defined by the k_{off} to k_{on} ratio, cannot be quantified separately; only the apparent equilibrium dissociation rate K_dV_r can be estimated.

APPENDIX B

Tracer kinetics analysis

CNL method. Parameters of the model was identified by minimization of a weighted least-squares cost function, using the Marquardt algorithm, knowing the labeled part of compartment concentrations with the PET measurements and the measured arterial function:

$$\mathbf{M^*_{PET}(t) = (1 - F_v)C^*_b(t) + M^*_{f+ns}(t) + M^*_s(t),}$$

where F_v is the vascular fraction of blood present in the tissue volume, $M^*_{PET}(t)$ is the local time-concentration curve measured by PET, and $C^*_b(t)$ is the time-concentration curve measured in whole blood. $M^*_{f+ns}(t)$ and $M^*_s(t)$ denote the labeled quantity of $M_{f+ns}(t)$ and $M_s(t)$.

Because linear differential equations are ruling the link between $C_a(t)$, $M_{f+ns}(t)$, and $M_s(t)$, the system could be solved by knowing $M^*_{PET}(t)$, $C^*_b(t)$.

In this model, we assume that metabolites of [^{18}F]MPPF do not cross the brain-blood barrier, as it is supported by *ex vivo* findings in the rat (Plenevaux et al., 2000*b*).

Logan method. In the Logan-Patlak graphical method, the slope of the asymptote for the graphic projection of data represents the total DV of the tracer in the region (V_t^L). From this slope, under the assumption that V_2 is equivalent in both regions, a BP of the equation can be evaluated with the ratio between the asymptote slope of a target region and the asymptote slope of a reference tissue:

$$BP^L = \frac{V_{t\ target}^{L}}{V_{t\ reference}^{L}} - 1 \qquad (1)$$

APPENDIX C

Parameter comparison

The relation between parameters of these two approaches is based on the following definitions. The total DV (V_t) is an equilibrium constant reached when the exchanges between the arterial and the tissue compartments are equilibrated (Mintun et al., 1984). The total DV (V_t) is the sum of the DV of the free and nonspecific compartment V_2 , and the DV of specific-compartment V_3. From the compartment model and the definition of the exchange rate, the relations between parameters can be established by the following equations (Koeppe et al, 1991):

$$V_2 = \frac{K_1}{k_2} \qquad (2)$$

$$V_3 = \frac{K_1}{k_2}\frac{k_3}{k_4} = \frac{K_1}{k_2}\frac{(k_{on}/V_r)B_{max}}{k_{off}} \qquad (3)$$

Because in the case of specific binding to receptor $k_3 = k_{on} \cdot B_{max}/V_r$, then the total volume of distribution is:

$$V_t = \frac{K_1}{k_2}\left(1 + \frac{k_{on}B_{max}}{V_r k_{off}}\right) \qquad (4)$$

The BP (defined as the quotient B_{max} and K_D) can also be analytically linked to the model parameters with the following equation:

$$BP = \frac{(k_{on}/V_r)B_{max}}{k_{off}} \qquad (5)$$

The parameter BP^L defined in the Logan method can also be analytically evaluated with the following formula:

$$BP^L{}_{analytic} = \frac{V_{t\ target}}{V_{t\ reference}} - 1 \qquad (6)$$

where $V_{t\ target}$ is the total DV in the target region, and $V_{t\ reference}$ is the total DV in the region taken as reference, computed with Eq. 4.

ACKNOWLEDGMENTS

The authors thank V. Berthier, M. Li-onnet, and C. Vighi, for excellent medical assistance during the PET experiment, G. Bonmarchand for [^{18}F] MPPF syntheses, S. Guillouet and F. Bonnefoi for chemical assistance and blood sample analyses, and Dr. Marc Hermier for providing access to the MR image acquisition and for taking medical responsibility of the MR imaging session.

REFERENCES

Brix G, Zaers J, Adam LE, Bellemann ME, Ostertag H, Trojan H, Haberkorn U, Doll J, Oberdorfer F, Lorenz WJ (1997) Performance evaluation of a whole-body PET scanner using the NEMA protocol. National Electrical Manufacturers Association. *J Nucl Med* 38:1614-1623

Burnet PW, Eastwood SL, Harrison PJ (1997) [3H]WAY-100635 for 5-HT1A receptor autoradiography in human brain: a comparison with [3H]8-OH-DPAT and demonstration of increased binding in the frontal cortex in schizophrenia. *Neurochem Int* 30:565-574

Chugani DC, Muzik O, Chakraborty P, Mangner T, Chugani HT (1998) Human brain serotonin synthesis capacity measured *in vivo* with alpha-[C-ll]methyl-L-tryptophan. *Synapse* 28:33-43

Cliffe IA (2000) A retrospect on the discovery of WAY-100635 and the prospect for improved 5-HT(lA) receptor PET radioligands. *Nucl Med Biol* 27:441-447

Cowen PJ (2000) Psychopharmacology of 5-HT(lA) receptors. *Nucl Med Biol* 27:437-439

Delforge J, Syrota A, Mazoyer BM (1989) Experimental design optimisation: theory and application to estimation of receptor model parameters using dynamic positron emission tomography. *Phys Med Biol* 34:419-435

Delforge J, Syrota A, Mazoyer BM (1990) Identifiability analysis and parameter identification of an *in vivo* ligand-receptor model from PET data. *IEEE Trans Biomed Eng* 37:653-661

Delforge J, Pappata S, Millet P, Samson Y, Bendriem B, Jobert A, Crouzel C, Syrota A (1995) Quantification of benzodiazepine receptors in human brain using PET, [^{11}C]flumazenil, and a single-experiment protocol. *J Cereb Blood Flow Metab* 15:284-300

Delforge J, Syrota A, Bendriem B (1996) Concept of reaction volume in the *in vivo* ligand-receptor model [see comments]. *J Nucl Med* 37:118-125

Farde L, Ito H, Swahn CG, Pike VW, Halldin C (1998) Quantitative analyses of carbonyl-carbon-ll-WAY-100635 binding to central 5-hydroxytryptamine-1A receptors in man. *J Nucl Med* 39:1965-1971

Ginovart N, Hassoun W, Le Bars D, Weissmann D, Leviel V (2000) *In vivo* characterization of p-[(18)F]MPPF, a fluoro analog of WAY-100635 for visualization of 5-HT(la) receptors. *Synapse* 35:192-200

Gunn RN, Sargent PA, Bench CJ, Rabiner EA, Osman S, Pike VW, Hume SP, Grasby PM, Lammertsma AA (1998) Tracer kinetic modeling of the 5-HT1A receptor ligand [carbonyl-^{11}C]WAY-100635 for PET. *Neuroimage* 8:426-440

Hall H, Lundkvist C, Halldin C, Farde L, Pike VW, McCarron JA, Fletcher A, Cliffe IA, Barf T, Wikstrom H, Sedvall G (1997) Autoradiographic localization of 5-HT1A receptors in the postmortem human brain using [3H]WAY-100635 and [^{11}C]way-100635. *Brain Res* 745:96-108

Hume S, Hirani E, Opacka-Juffry J, Myers R, Townsend C, Pike V, Grasby P (2001) Effect of 5-HT on binding of [(^{11})C] WAY 100635 to 5-HT(IA) receptors in rat brain, assessed using *in vivo* microdialysis nd PET after fenfluramine. *Synapse* 41:150-159

Koeppe RA, Holthoff VA, Frey KA, Kilbourn MR, Kuhl DE (1991) Compartmental analysis of [^{11}C]flumazenil kinetics for the estimation of ligand transport rate and receptor distribution using positron emission tomography. *J Cereb Blood Flow Metab* 11:735— 744

Le Bars D, Lemaire C, Ginovart N, Plenevaux A, Aerts J, Brihaye C, Hassoun W, Leviel V, Mekhsian P, Weissmann D, Pujol JF, Luxen A, Comar D (1998) High-yield radiosynthesis and preliminary *in vivo* evaluation of p-[18F]MPPF, afluoro analog of WAY-100635. *Nucl Med Biol* 25:343-350

Le Bars D, Bonmarchand G, Alvarez G, Lemaire C, Mosdzianowski C (2001) New automation of MPPF using a coincidence synthesizer: 14th International Symposium on Radiopharmaceuticals. *J Labeled Cpd Radiopharm,* 44:sl045-sl046

Logan J, Fowler JS, Volkow ND, Wolf AP, Dewey SL, Schlyer DJ, MacGregor RR, Hitzemann R, Bendriem B, Gatley SJ, et al. (1990) Graphical analysis of reversible radioligand binding from time-activity measurements applied to [N-l lC-methyl]-(-)-cocaine PET studies in human subjects. *J Cereb Blood Flow Metab* 10:740-747

Louw D, Sutherland GR, Glavin GB, Girvin J (1989) A study of monoamine metabolism in human epilepsy. *Can J Neurol Sci* 16: 394-397

Mintun MA, Raichle ME, Kilbourn MR, Wooten GF, Welch MJ (1984) A quantitative model for the *in vivo* assessment of drug binding sites with positron emission tomography. *Ann Neurol* 15:217-227

Passchier J, van Waarde A, Pieterman RM, Elsinga PH, Pruim J, Hen-drikse HN, Willemsen AT, Vaalburg W (2000*a*) *In vivo* delineation of 5-HT1A receptors in human brain with [18F]MPPF. *J Nucl Med* 41:1830-1835

Passchier J, van Waarde A, Pieterman RM, Elsinga PH, Pruim J, Hen-drikse HN, Willemsen AT, Vaalburg W (2000b) Quantitative imaging of 5-HT(lA) receptor binding in healthy volunteers with [(18)f]p-MPPF. *Nucl Med Biol* 27:473-476

Passchier J, van Waarde A, Vaalburg W, Willemsen AT (2001) On the quantification of [18F]MPPF binding to 5-HT1A receptors in the human brain. *J Nucl Med* 42:1025-1031

Peroutka SJ (1995) 5-HT receptors: past, present and future. *Trends Neurosci* 18:68-69

Pike VW, McCarron JA, Lammerstma AA, Hume SP, Poole K, Grasby

PM, Malizia A, Cliffe IA, Fletcher A, Bench CJ (1995) First delineation of 5-HT1A receptors in human brain with PET and [^{n}C]WAY-100635. *Eur J Pharmacol* 283:Rl-3

Pike VW, McCarron JA, Lammertsma AA, Osman S, Hume SP, Sargent PA, Bench CJ, Cliffe IA, Fletcher A, Grasby PM (1996) Exquisite delineation of 5-HT1A receptors in human brain with PET and [carbonyl-11 C]WAY-100635. *Eur J Pharmacol* 301:R5-R7

Pintor M, Mefford IN, Hutter I, Pocotte SL, Wyler AR, Nadi NS (1990) Levels of biogenic amines, their metabolites, and tyrosine hydroxylase activity in the human epileptic temporal cortex. *Synapse* 5:152-156

Plenevaux A, Lemaire C, Aerts J, Lacan G, Rubins D, Melega WP, Brihaye C, Degueldre C, Fuchs S, Salmon E, Maquet P, Laureys S, Damhaut P, Weissmann D, Le Bars D, Pujol J, Luxen A (2000*a*) [(18)F]p-MPPF: A radiolabeled antagonist for the study of 5-HT(lA) receptors with PET [In Process Citation]. *Nucl Med Biol* 27:467-471

Plenevaux A, Weissmann D, Aerts J, Lemaire C, Brihaye C, Degueldre C, Le Bars D, Comar D, Pujol J, Luxen A (2000*b*) Tissue distribution, autoradiography, and metabolism of 4-(2'-methoxyphenyl)-1 -[2' -[N-2'-pyridinyl)-p-[(18)F]fluorobenzami-do]ethyl]piperazine (p-[(18)F]MPPF), a new serotonin 5-HT(lA) antagonist for positron emission tomography: an *in vivo* study in rats. *J Neurochem* 75:803-811

Statnick MA, Dailey JW, Jobe PC, Browning RA (1996) Abnormalities in 5-HT1A and 5-HT1B receptor binding in severe-seizure genetically epilepsy-prone rats (GEPR-9s). *Neuropharmacology* 35:111— 118

Wada Y, Shiraishi J, Nakamura M, Koshino Y (1997) Role of serotonin receptor subtypes in the development of amygdaloid kindling in rats. *Brain Res* 747:338-342

Woods RP, Cherry SR, Mazziotta JC (1992) Rapid automated algorithm for aligning and reslicing PET images. *J Comput Assist Tomogr* 16:620-633.

Woods RP, Mazziotta JC, Cherry SR (1993) MRI-PET registration with automated algorithm. *J Comput Assist Tomogr* 17:536-546

Zhuang ZP, Kung MP, Chumpradit S, Mu M, Kung HF (1994) Derivatives of 4-(2'-methoxyphenyl)-l-[2'-(N-2''-pyridinyl-p-iodobenzamido)ethyl]pipera zine (p-MPPI) as 5-HT1A ligands. *J Med Chem* 37:4572-4575.